Research Article

Shi-Yan Cheah, Mohammod Aminuzzaman, You-Kang Phang, Sharon Chia-Yen Lim, Ming-Xiu Koh, Sinouvassane Djearamane, Hemaroopini Subramaniam, Boon-Hoe Lim, Fang Li, Ling-Shing Wong*, and Lai-Hock Tey*

Green-synthesized chromium oxide nanoparticles using pomegranate husk extract: Multifunctional bioactivity in antioxidant potential, lipase and amylase inhibition, and cytotoxicity

https://doi.org/10.1515/gps-2024-0246
received November 28, 2024; accepted May 04, 2025

Abstract: Malnutrition is a growing global health concern that contributes to obesity. This study presents the green synthesis of chromium oxide nanoparticles (Cr_2O_3 NPs) using pomegranate husk aqueous extract as both reducing and capping agents via a microwave-assisted method. The synthesized MA-Cr_2O_3 NPs were characterized using UV-Vis, FTIR, field emission scanning electron microscope, energy dispersive X-ray (EDX), HR-transmission electron microscopy (TEM), and X-ray diffraction methods. TEM analysis revealed an average particle size of 11.69 nm, and EDX confirmed nanoparticle (NP) purity. Antioxidant activity was assessed through 2,2′-diphenyl-1-picrylhydrazyl and ABTS assays, showing strong free radical scavenging abilities of 80.4% and 65.8% at 1 and 5 $mg{\cdot}mL^{-1}$, respectively. The NPs also contained notable levels of phenolics (10.14 mg $GAE{\cdot}g^{-1}$) and flavonoids (33.28 mg $QE{\cdot}g^{-1}$). In enzyme inhibition assays, NPs exhibited potent activity against pancreatic lipase (91.7%) and α-amylase (90.5%), with EC_{50} values of 0.16 ± 0.002 $mg{\cdot}mL^{-1}$ and 0.15 ± 0.003 $mg{\cdot}mL^{-1}$ at 0.25 $mg{\cdot}mL^{-1}$. Cytotoxicity testing on Vero cells showed 55.5% viability at 0.25 $mg{\cdot}mL^{-1}$, indicating acceptable biocompatibility. These results highlight the potential of MA-Cr_2O_3 NPs for antioxidant and anti-obesity applications, offering a sustainable and eco-friendly solution for managing health issues related to malnutrition.

Keywords: obesity, Cr_2O_3 nanoparticles, green synthesis, enzyme inhibition, biocompatibility

1 Introduction

Obesity is recognized as a chronic condition marked by an imbalance between energy intake and expenditure, resulting in excessive fat accumulation [1]. The global prevalence of obesity has increased substantially, with the World Health Organization indicating that by 2022, 60% of the European population will be classified as overweight or obese [2]. Obesity is a significant risk factor for various metabolic disorders, such as cardiovascular disease (CVD), hypertension, and diabetes mellitus [3,4]. Traditional anti-obesity interventions, including lifestyle changes, pharmacological treatments, and surgical procedures, often have limitations due to potential side effects, invasiveness, or issues with long-term sustainability [5]. Pharmacological treatments commonly lead to adverse reactions, including nausea, vomiting, fecal urgency, and oily stools, while surgical approaches like liposuction and bariatric surgery are often followed by the risk of weight regain [6,7]. These challenges have driven researchers to explore alternative approaches, such as enzyme inhibition, which targets metabolic processes directly related to obesity, for potentially safer and more effective treatment options.

In recent years, metal nanoparticles (NPs) have emerged as promising agents in obesity research due to their unique physicochemical properties, such as high surface area, catalytic potential, and bioavailability. NPs, typically defined as

* **Corresponding author: Ling-Shing Wong,** Faculty of Health and Life Sciences, INTI International University, Nilai, 71800, Malaysia, e-mail: lingshing.wong@newinti.edu.my
* **Corresponding author: Lai-Hock Tey,** Department of Chemical Science, Faculty of Science, Universiti Tunku Abdul Rahman (UTAR), Kampar Campus, Kampar, Perak, Malaysia, e-mail: teylh@utar.edu.my
Shi-Yan Cheah, Mohammod Aminuzzaman, You-Kang Phang, Sharon Chia-Yen Lim, Ming-Xiu Koh, Boon-Hoe Lim: Department of Chemical Science, Faculty of Science, Universiti Tunku Abdul Rahman (UTAR), Kampar Campus, Kampar, Perak, Malaysia
Sinouvassane Djearamane, Hemaroopini Subramaniam: Department of Allied Health Sciences, Faculty of Science, Universiti Tunku Abdul Rahman (UTAR), Kampar Campus, Kampar, Perak, Malaysia
Fang Li: School of Pharmacy, Jiangsu Vocational College of Medicine, Yancheng 224005, China

particles smaller than 100 nm, have become prominent in nanotechnology due to their distinctive physicochemical properties and promising applications in biomedicine [8,9]. Metal oxide NPs, chromium oxide nanoparticles (Cr_2O_3 NPs), stand out among various metal oxides due to their unique properties, including exceptional thermal stability, magnetic behavior, biocompatibility, and diverse biological activities, including antioxidant, anti-inflammatory, and enzyme-inhibitory properties. These characteristics make Cr_2O_3 NPs promising candidates for diverse applications, such as in catalysis, environmental remediation, antimicrobial activity, and therapeutic treatments [10].

The synthesis of Cr_2O_3 NPs through green approaches offers an eco-friendly alternative to conventional chemical processes, which often involve hazardous chemicals and generate harmful by-products [11,12]. Pomegranate husk (*Punica granatum*), an agricultural byproduct, contains a rich composition of polyphenols, flavonoids, tannins, and other bioactive compounds that exhibit reducing and stabilizing properties, making it an excellent choice for NP synthesis. The utilization of pomegranate husk not only aligns with principles of waste valorization but also promotes a circular economy by repurposing waste materials for valuable applications. Moreover, pomegranate husk extracts (PHEs) are known for their antioxidant, antimicrobial, and anti-inflammatory activities, further enhancing the multifunctional properties of the synthesized NPs. In this study, pomegranate husk is utilized as a natural reducing and stabilizing agent for synthesizing Cr_2O_3 NPs through a microwave-assisted technique [13]. This technique provides fast and even heating, enabling the production of uniform NPs more effectively than traditional heating methods [14]. The synthesized NPs were thoroughly characterized to assess their structural, chemical, and morphological properties. Additionally, their antioxidant activity, enzyme inhibition potential, and cytotoxicity were evaluated to explore their suitability for use in combating obesity and its associated health risks.

Chromium (Cr) plays an essential role in glucose metabolism and lipid processing, with its trivalent form (Cr^{3+}) being the most stable and least toxic [15–17]. This study examines the antioxidant potential and inhibitory effects of Cr_2O_3 NPs on pancreatic lipase and α-amylase. Pancreatic lipase is a critical enzyme in fat digestion, responsible for converting 50–70% of dietary lipids into fatty acids and glycerols, while α-amylase facilitates the breakdown of complex polysaccharides into simpler carbohydrates in the small intestine [18–20]. High sugar intake can increase glucose and fructose levels in the bloodstream, stimulating lipogenesis and causing lipid storage in white adipose tissue, which may contribute to obesity [21,22]. Furthermore, oxidative stress – an imbalance between reactive oxygen species (ROS) and antioxidants – has been associated with obesity through processes like mitochondrial dysfunction, lipid storage, insulin resistance, and inflammation [23–25].

This study explores Cr_2O_3 NPs synthesized using PHEs, which show promise in tackling obesity due to their antioxidant effects and potential to inhibit enzymes. The cytotoxicity of these NPs is evaluated on Vero cells, a cell line from the African green monkey kidney, to ensure their safety and biocompatibility for therapeutic use. The study aims to investigate the multifunctional bioactivity of the green-synthesized Cr_2O_3 NPs, providing a sustainable and effective strategy for addressing obesity and its associated complications.

2 Materials and methods

2.1 Materials

The pomegranate husk was collected from Kampar, Malaysia. Chromium(III) nitrate nonahydrate [$Cr(NO_3)_3{\cdot}9H_2O$], sodium carbonate, sodium hydroxide, 95% ethanol, gallic acid, ascorbic acid, and quercetin hydrate were purchased from Synertec Enterprise (Malaysia). The chemicals and consumables used for MTT assay, such as Dulbecco's modified Eagle's medium (DMEM), were purchased from Medigene (Malaysia). Lipase from porcine pancreas, α-amylase from porcine pancreas, 4-nitrophenyl palmitate (p-NPP), ABTS, DPPH (2,2-diphenyl-1-picrylhydrazyl), Orlistat, and Acarbose were purchased from Medigene (Malaysia). All chemicals used were of analytical or reagent grade.

2.2 Preparation of PHE

The extraction started with separating the pomegranate husk from the seed. Then, the pomegranate husk was cleaned and cut into pieces. Then, 100 g of cut pomegranate husk was added to 150 mL of deionized water and heated at 70°C for 30 min. The PHE was filtered using Whatman No. 1 filter paper thrice to obtain a clear PHE solution. The PHE was stored at 4°C until further use.

2.3 Microwave-assisted green synthesis of Cr_2O_3 NPs (MA-Cr_2O_3 NPs)

Figure 1 illustrates the microwave-assisted green synthesis of Cr_2O_3 NPs. First, 3 g of chromium(III) nitrate nonahydrate

salt was mixed with 50 mL of PHE under stirring conditions at room temperature for 5 min. Then, a microwave synthesizer (CEM Corporator) was used for the synthesizing process at 60°C in high stirring mode for 30 min. After that, rotary evaporation (Heidolph 5 L) was applied until a dark green paste was obtained. The dark green paste was calcinated at 450°C for 2 h, and a dark green powder was obtained. Finally, the dark green Cr_2O_3 powder was ground using a pestle and mortar and stored in an airtight container for further use [26].

2.4 Characterizations

The absorption peaks were measured in the ultraviolet and visible regions using a UV-VIS Spectrophotometer (Genesys 10 S UV-VIS), which ranged from 200 to 800 nm in scanning mode. The surface morphology, size, and elemental compositions were determined using a field emission scanning electron microscope (FE-SEM) (JOEL JSM 6701-F) with energy dispersive X-ray analysis (EDX) (X-max, 150-Oxford Instruments) and transmission electron microscope (HR-TEM, JOEL JEM-2100F). Besides, the functional groups were determined using FTIR spectroscopy (Perkin Elmer Spectrum EX1) using the KBr pellet method in the range of 4,000–400 cm^{-1}. X-ray diffraction (XRD) (Shidmazu 6000) characterization was carried out to determine the crystallinity of the NPs in the range of 20–80°.

2.5 Antioxidant capacity

2.5.1 Total phenolic content (TPC)

The TPC of the microwave-assisted green-synthesized Cr_2O_3 NPs and PHE was determined using the Folin–Ciocalteu method. To begin, 0.1 mL of each sample was combined with 0.75 mL of 10-fold diluted Folin–Ciocalteu reagent. The mixture was incubated in the dark for 5 min, after which 0.75 mL of 6% sodium carbonate solution was added. The mixture was then incubated again in the dark for 90 min. Finally, the absorbance was measured at 725 nm using a UV-Vis spectrophotometer (Genesys 10 S UV-VIS), with gallic acid (0–0.2 $mg{\cdot}mL^{-1}$) serving as the standard reference [27].

2.5.2 Total flavonoid content (TFC)

The TFC of the microwave-assisted green-synthesized Cr_2O_3 NPs and PHE was determined using the aluminum colorimetric method. Initially, 0.2 mL of each sample was mixed with 5% sodium nitrite and incubated for 6 min. Following this, 0.15 mL of 10% aluminum chloride was added and incubated for 6 min. Subsequently, 10% sodium hydroxide was added, followed by a final incubation for 15 min. The absorbance was then recorded at 510 nm using a UV-Vis spectrophotometer (Genesys 10 S UV-VIS), with quercetin hydrate (99%) at concentrations ranging from 0 to 0.2 $mg{\cdot}mL^{-1}$ serving as the standard reference [27].

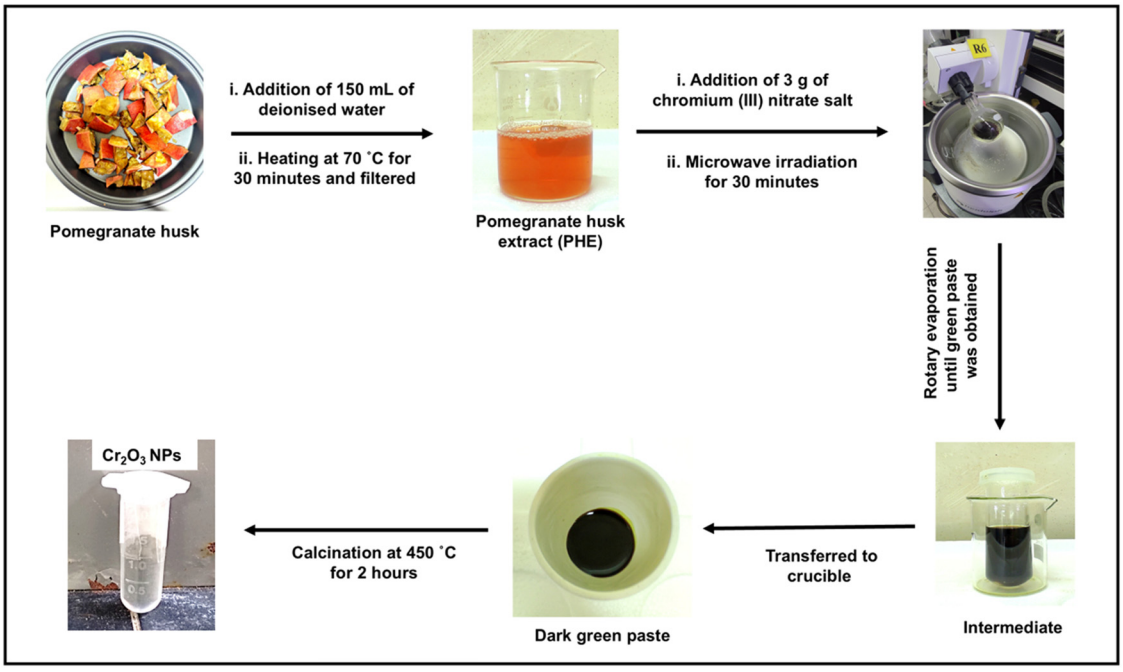

Figure 1: Green synthesis of Cr_2O_3 NPs using a microwave-assisted method.

2.6 Free radical scavenging activity

2.6.1 DPPH assay

DPPH assay was performed, as described in the referenced method, to evaluate the free radical scavenging activity of MA-Cr_2O_3 NPs and PHE. A stock solution of DPPH was initially prepared by dissolving DPPH powder in 95% ethanol. The stock solution was then diluted with ethanol to achieve a working solution with an absorbance of 0.98 ± 0.02 Au. For the assay, 0.2 mL of each sample (0–1 mg·mL^{-1}) was mixed with 1 mL of the DPPH working solution and incubated in the dark for 30 and 60 min. Absorbance was measured at 517 nm using a UV-Vis spectrophotometer (Genesys 10 S UV-VIS), with ascorbic acid (0–0.12 mg·mL^{-1}) used as the reference standard [28].

2.6.2 ABTS (2,2'-azino-bis (3-ethylbenzothiazoline-6-sulfonic acid)) assay

The ABTS assay was performed according to established protocols [29]. To prepare the ABTS stock solution, ABTS was mixed with potassium persulfate at concentrations of 7.4 mM and 2.4 mM, respectively, and allowed to incubate in the dark for 12–16 h. The stock solution was then diluted to create the ABTS working solution, adjusted to an absorbance of 0.70 ± 0.02 Au. For the assay, 0.2 mL of each sample (0–5 mg·mL^{-1}) was combined with 1 mL of the ABTS working solution and incubated in the dark for 10, 20, and 30 min. Absorbance was subsequently measured at 734 nm using a UV-Vis spectrophotometer (Genesys 10 S UV-VIS), with butylated hydroxytoluene (0–0.12 mg·mL^{-1}) serving as the reference standard.

The percentage of free radical scavenging activities was calculated using the following equation:

$$\text{Free radical scavenging} = \frac{\text{Abs of control} - \text{Abs of sample}}{\text{Abs of control}} \times 100\%$$

where Abs of control represents the absorbance value of the control (DPPH or ABTS solution only), and Abs of the test sample represents the absorbance value of the test sample.

2.7 Enzyme inhibition

2.7.1 Pancreatic lipase inhibition

The pancreatic lipase inhibitory activity of MA-Cr_2O_3 NPs and PHE was evaluated using a slightly modified version of the method outlined in the study of Cam-Van et al. [30]. First, 0.3 mL of each sample (0.00–0.30 mg·mL^{-1}) was mixed with 1 mL of pancreatic lipase (prepared in 0.1 M buffer) and incubated at 37°C for 15 min. Following this, 0.3 mL of p-NPP solution (dissolved in isopropanol) was added to the mixture. The reaction was then incubated for an additional 15 min at 37°C. Absorbance was measured at 405 nm using a UV-Vis spectrophotometer (Genesys 10 S UV-VIS), with Orlistat (0.00–0.12 mg·mL^{-1}) used as the reference standard [30].

2.7.2 α-Amylase inhibition

The α-amylase inhibition assay was conducted using the dinitrosalicylic acid method, as described by Akhter et al. [31], with minor modifications. Initially, 0.2 mL of each sample (0.00–0.30 mg·mL^{-1}) was combined with 1 mL of α-amylase solution (prepared in phosphate-buffered saline [PBS]) and incubated at 37°C for 10 min. After incubation, 0.2 mL of a 1% starch solution was added to the mixture, followed by a second incubation period. To terminate the reaction, 0.5 mL of 3,5-dinitrosalicylic acid solution was added, and the mixture was heated in a boiling water bath for 5 min. Finally, the absorbance was recorded at 540 nm using a UV-Vis spectrophotometer (Genesys 10 S UV-VIS), with acarbose (0.00–0.12 mg·mL^{-1}·mL^{-1}) serving as the reference standard [31].

The percentage of enzymatic inhibition was calculated using the following equation:

$$\text{Enzymatic inhibition} = \frac{\text{Abs of sample} - \text{Abs of control}}{\text{Abs of sample}} \times 100\%$$

where Abs of sample represents the absorbance value of the test sample, and Abs of control represents the absorbance value of enzymatic control (enzyme and substrate only).

2.8 Cytotoxicity test

2.8.1 Cell culture

Vero cells (ATCC CCL-81) were passaged and prepared for the 3-(4,5-dimethylthiazol-2-yl)-2,5-diphenyltetrazolium bromide (MTT) assay. All procedures were performed in a laminar flow hood. To sub-culture the cells, the medium was discarded from the culture flask, and 5 mL of PBS was pipetted in to wash away any impurities. Then, 3 mL of trypsin-EDTA was added to the flask and incubated for 15 min at 37°C. After the incubation, the reaction was terminated by adding 3 mL of complete growth medium (CGM). The cell suspension was then centrifuged at 1,000 rpm for 10 min at room temperature. Finally, 2 mL of CGM was added to two separate new culture flasks, respectively [32].

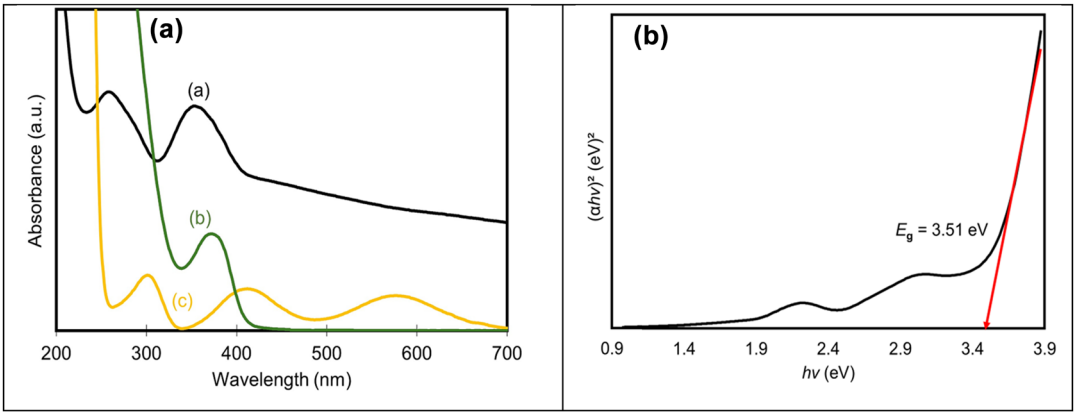

Figure 2: UV-Vis spectra of (a) Cr_2O_3 NPs, (b) chromium nitrate salt solution, and (c) PHE. (b) Energy bandgap of Cr_2O_3 NPs.

2.8.2 MTT assay

The seedling process was similar to the sub-culture procedure described earlier. After centrifugation, 2 mL of DMEM) was added to a centrifuge tube, gently mixed, and transferred to a reservoir pre-loaded with DMEM. Then, 0.1 mL of the solution was added to the 96-well plate according to the experimental design, with DMEM used for the blank wells. The 96-well plate was incubated at 37°C for 24 h.

To prepare the stock solution of NPs, 1 mg·mL^{-1} NPs was dissolved in PBS and filtered. This stock solution was then diluted to 0.25 mg·mL^{-1} and topped up with DMEM. Afterward, 100 µL of

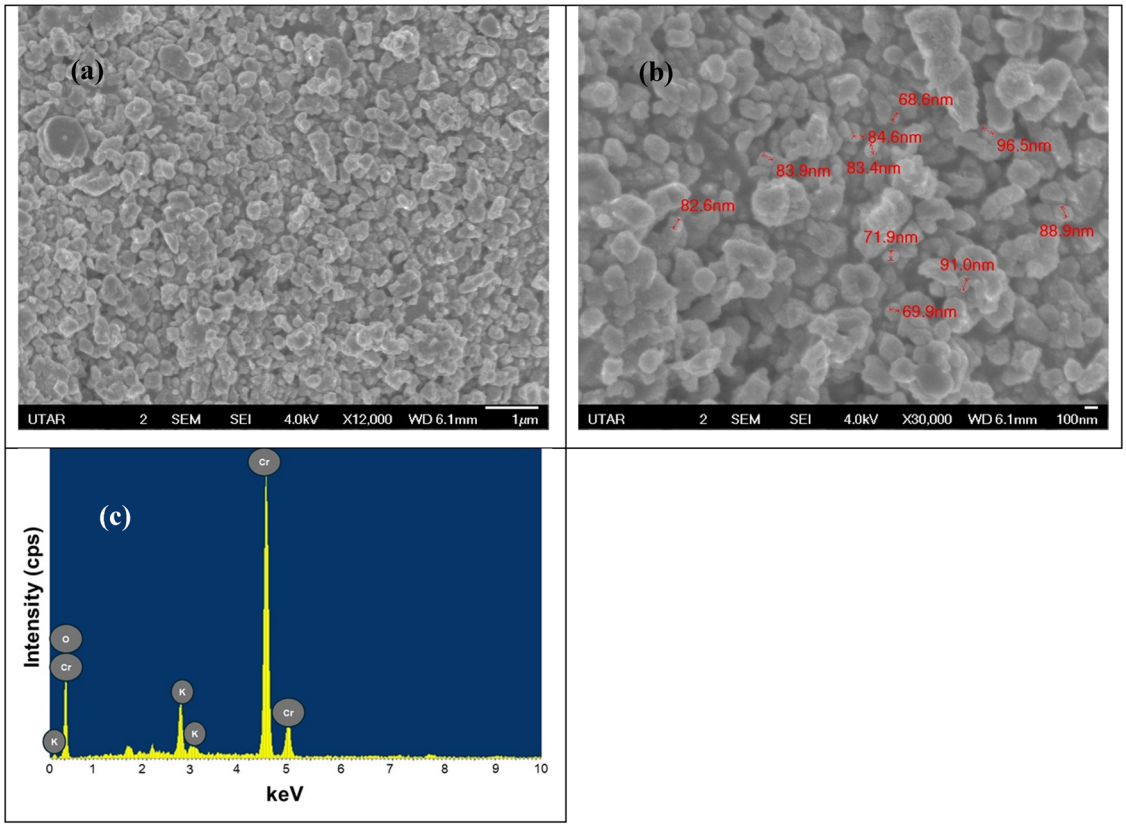

Figure 3: FE-SEM spectrum for MA-Cr_2O_3 NPs with the magnification at (a) 12,000×, scale bar = 1 µm; (b) 30,000×, scale bar = 100 nm. (c) EDX spectrum of MA-Cr_2O_3 NPs.

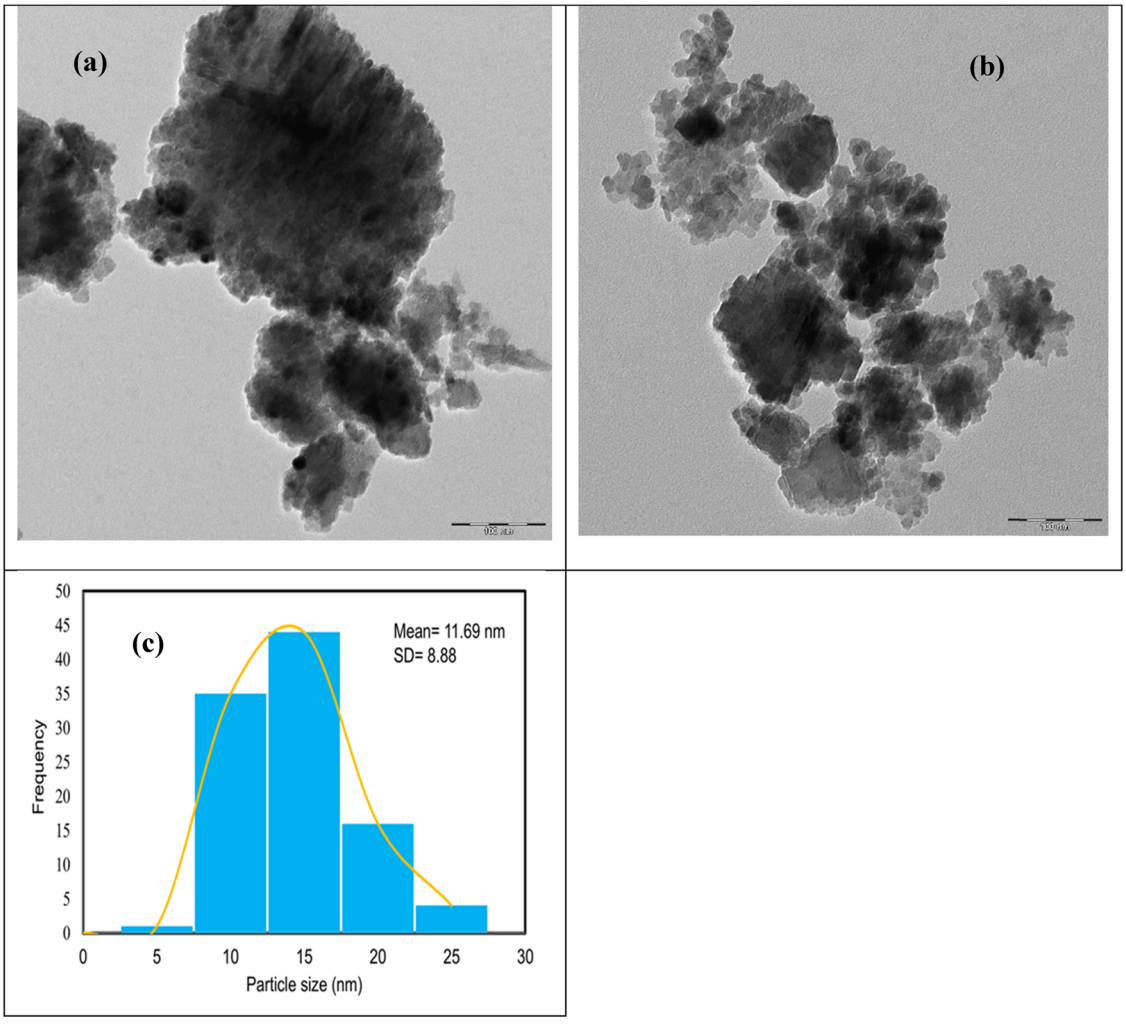

Figure 4: HR-TEM images of MA-Cr_2O_3 NPs at (a) scale bar = 100 nm and (b) scale bar = 100 nm. (c) Particle distribution of MA-Cr_2O_3 NPs.

the NP solution was added to each well of the 96-well plate according to the experiment design, and the plate was incubated at 37°C for 24 h. DMSO was used as the reference standard.

The MTT reagent was prepared in PBS under dark conditions and placed in a 37°C water bath for 15 min. Then, 0.02 mL of MTT reagent was added to each well, and the plate was incubated for 4 h. After incubation, the solution in each well was discarded, and 100 µL of DMSO was added to each well. The absorbance was measured at 570 nm using UV-Vis (Genesys 10 S UV-VIS) [33].

The percentage of cell viability was calculated using the following equation:

$$\text{Cell viability} = \frac{\text{Abs of sample} - \text{Abs of blank}}{\text{Abs of control} - \text{Abs of blank}} \times 100$$

where Abs of sample represents the absorbance value of the test sample, Abs of blank represents the absorbance value of the blank (only DMEM solution), and Abs of control represents the absorbance value of the control.

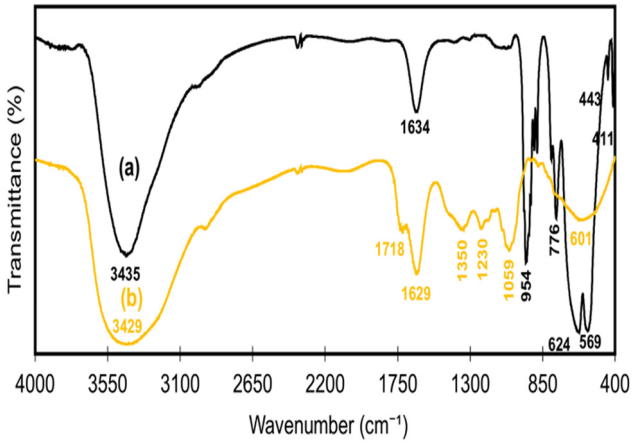

Figure 5: FTIR spectra of (a) MA-Cr_2O_3 NPs and (b) PHE.

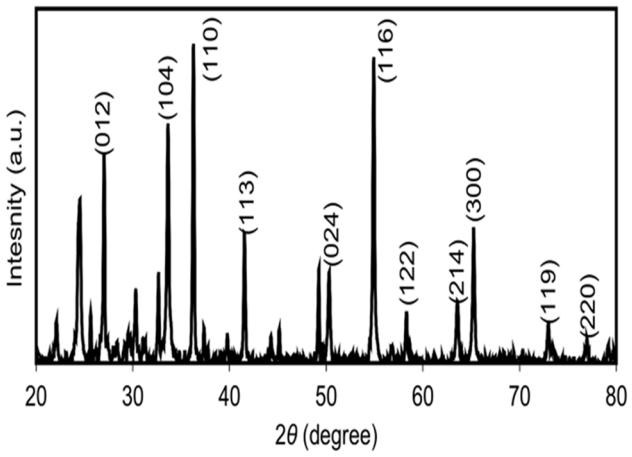

Figure 6: XRD spectrum of MA-Cr_2O_3 NPs.

2.9 Statistical analysis

All data were collected in triplicate ($n = 3$), and the results are presented as mean ± standard error. Statistical differences were analyzed using one-way ANOVA followed by a *t*-test, with $p < 0.05$ considered significant.

3 Results and discussion

3.1 Characterizations

UV-VIS characterization was performed using 0.1 mg·mL^{-1} MA-Cr_2O_3 NPs, PHE, and a chromium nitrate(III) nonahydrate salt solution. Figure 2(a) displays the UV-VIS spectrum for the microwave-assisted green synthesis of Cr_2O_3 NPs. The MA-Cr_2O_3 NPs exhibited absorption peaks at 258 and 354 nm, which align with previously reported findings [34]. The energy bandgap in Figure 2(b) from the UV-VIS analysis was determined to be 3.51 eV. The two observed absorption peaks corresponding to the 4A2g → 4T1g and 4A2g → 4T2g transitions confirm the successful formation of Cr_2O_3 NPs [35]. Figure 3 shows the UV-VIS spectrum for PHE, with absorption peaks at 257 and 373 nm. These peaks are associated with the presence of secondary metabolites like polyphenolic compounds, anthocyanins, and tannins [36]. The shifting of absorption peaks and the color change from PHE and chromium(III) nitrate nonahydrate to Cr_2O_3 NPs are attributed to surface plasmon resonance [37].

The surface morphology and size of MA-Cr_2O_3 NPs were analyzed using FE-SEM. Figure 3(a) and (b) presents SEM images of MA-Cr_2O_3 NPs, which indicate that Cr_2O_3 NPs are densely agglomerated and nearly spherical. This can be attributed to the high viscosity of the plant extract, the strong forces of attraction, oxidation of nanomaterials, and isotropic aggregation occurring at the isoelectric point [38,39]. The size of MA-Cr_2O_3 NPs is observed to range from 68 to 97 nm. Figure 3(c) displays the EDX spectrum of MA-Cr_2O_3 NPs, revealing the presence of chromium (Cr) (48.91%), oxygen (O) (44.52%), and potassium (K) (6.57%), indicating the high purity of the synthesized Cr_2O_3 NPs. The presence of potassium is likely due to the phytochemicals in the pomegranate husk, as suggested in the literature [40]. Figure 4(a) and (b) presents the HR-transmission electron microscopy (TEM) images of MA-Cr_2O_3 NPs, and the TEM histogram in Figure 4(c) indicates that the average size of the MA-Cr_2O_3 NPs is approximately 11.69 nm with the standard deviation of 8.88 and a size distribution range of 3–28 nm as observed from TEM analysis. The size of the

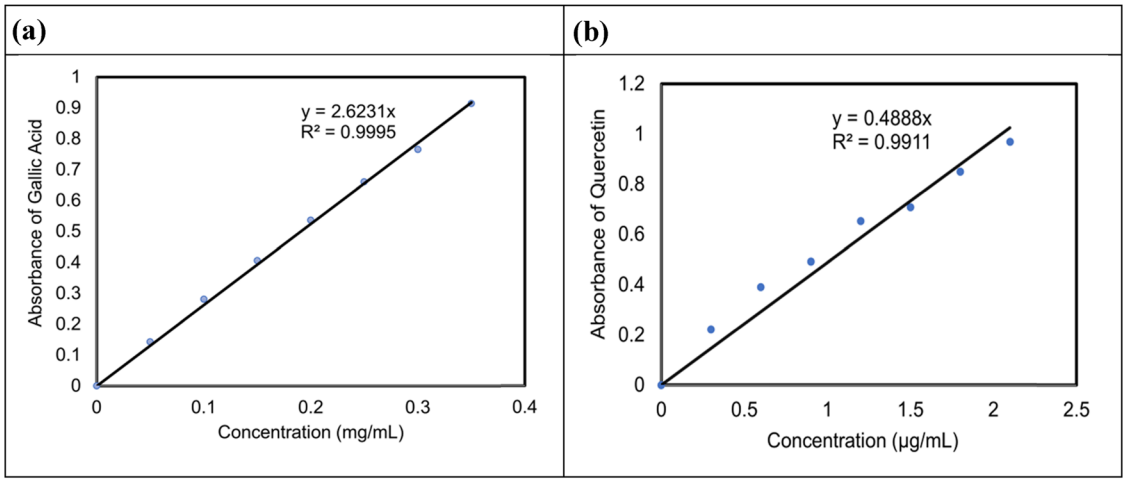

Figure 7: TPC for (a) gallic acid standard and TFC for (b) quercetin standard.

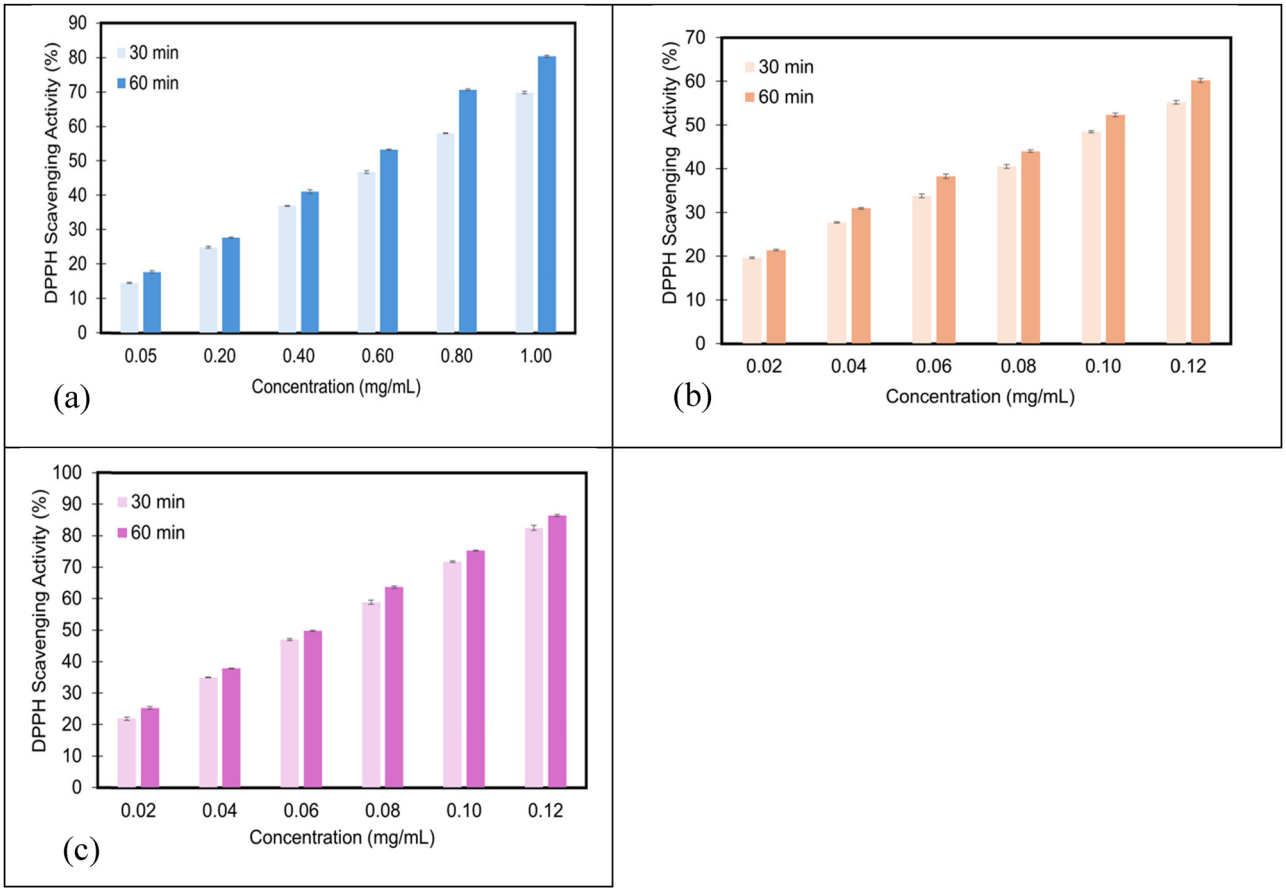

Figure 8: DPPH scavenging activity of (a) MA-Cr_2O_3 NPs, (b) PHE, and (c) ascorbic acid.

distribution is smaller as compared to the study using the conventional heating method, which shows that the sizes range from 35 to 60 nm [34]. Additionally, Cr_2O_3 NPs appear spherical and agglomerated, which is consistent with the FE-SEM observations.

Figure 5 displays the FTIR spectra for both MA-Cr_2O_3 NPs and PHE. The bands at 411, 443, 569, 624, 902, 924, 954, 1,045, and 1,077 cm^{-1} in the Cr_2O_3 NP spectrum correspond to the v(Cr–O) stretching vibrations [41–44]. The peaks at 776 and 879 cm^{-1} in PHE shifted to 766 and 884 cm^{-1} in Cr_2O_3 NPs, which are associated with v(C–H) bending modes [45]. Additionally, the bands at 1,629 cm^{-1} for PHE and 1,634 cm^{-1} for Cr_2O_3 NPs indicate moisture absorption on the surface, while the bands at 2,943 and 2,978 cm^{-1} correspond to sp^3 v(C–H) vibration modes from PHE [46]. The bands at 3,429 and 3,435 cm^{-1} indicate the presence of the O–H functional group due to moisture [47]. Some bands in PHE, such as those at 1,069, 1,147, 1,230, and 1,350 cm^{-1}, are absent in Cr_2O_3 NPs, possibly due to their removal during the calcination process at high temperatures [48]. Finally, weak peaks at 796, 2,345, and 2,370 cm^{-1} were observed in Cr_2O_3 NPs, while peaks at 1,718 and 2,371 cm^{-1} were observed for PHE.

Table 1: EC_{50} values for DPPH assays of MA-CR_2O_3 NPs, PHE, and standards

DPPH	EC_{50} ± SE (mg·mL^{-1}) (30 min)	EC_{50} ± SE (mg·mL^{-1}) (60 min)
MA-Cr_2O_3 NPs	0.66 ± 0.001	0.57 ± 0.002
PHE	0.01 ± 0.0003	0.099 ± 0.0005
Ascorbic acid	0.069 ± 0.0004	0.065 ± 0.0002

*This study was conducted in triplicate, with 30 and 60 min incubation.

Figure 6 presents the XRD spectrum for MA-Cr_2O_3 NPs. The diffraction peaks observed at 22.08°, 24.50°, 33.62°, 36.25°, 41.53°, 50.21°, 54.88°, 58.61°, 63.52°, 65.21°, 73.12°, 76.91°, and 79.2° are attributed to the (0 1 2), (0 1 2), (1 0 4), (1 1 0), (1 1 3), (0 2 4), (1 1 6), (1 2 2), (2 1 4), (3 0 0), (1 1 9), (2 2 0), and (3 0 6) lattice planes, as referenced in the ICDD database, entry number 01-084-1616 [49]. The XRD data indicate that MA-Cr_2O_3 NPs exhibit a trigonal (hexagonal axes) crystal structure, with unit cell dimensions of a = 4.9516 Å and c = 13.5987 Å. Additionally, the purity of

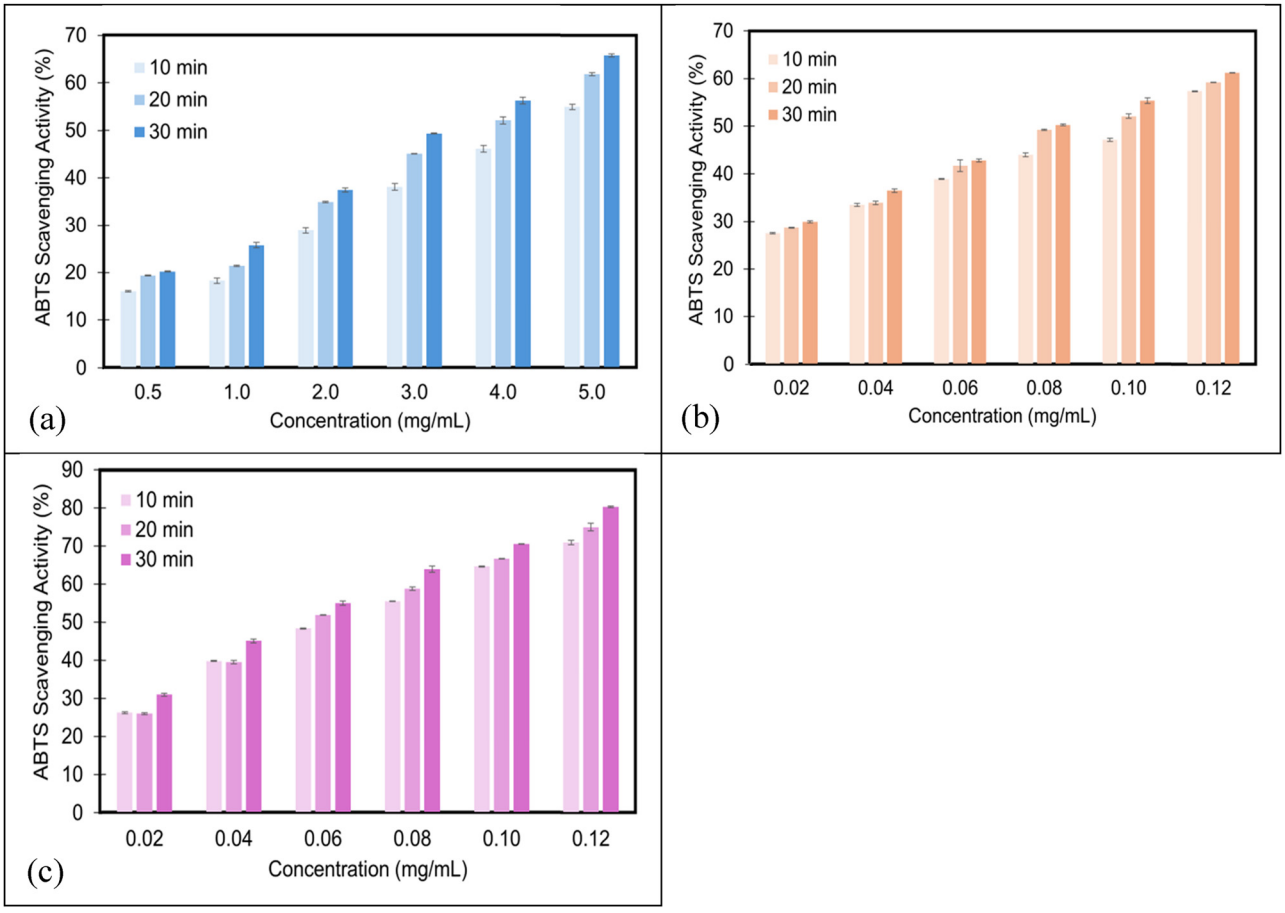

Figure 9: ABTS scavenging activity of (a) MA-Cr_2O_3 NPs, (b) PHE, and (c) BHT.

MA-Cr_2O_3 NPs is found to be 95.2%, with a degree of crystallinity of 10.68%. The crystalline size (D) of MA-Cr_2O_3 NPs was calculated using the Debye–Scherrer equation [50].

3.2 Antioxidant capacity

Phenolic and flavonoid contents found in the plant extracts are secondary metabolites produced by plants to defend themselves in their natural environment [51]. The hydroxyl groups present in phenolic compounds contribute to their free radical scavenging activity [52]. Flavonoids, which are derivatives of phenolic compounds, exhibit strong biomedical properties and are highly effective in antioxidant activities [53]. The TPC and TFC of MA-Cr_2O_3 NPs and PHE were assessed using the Folin–Ciocalteu and aluminum chloride calorimetry methods. Figure 7 shows the TPC and TFC graphs for the standards. PHE demonstrated high TPC and TFC values of 71.54 mg GAE·g^{-1} and 100.76 mg QE·g^{-1}, respectively, followed by MA-Cr_2O_3 NPs with 10.14 mg GAE·g^{-1} and 33.28 mg QE·g^{-1}. Studies have indicated that the lower TPC and TFC values in NPs compared to the plant extract are due to the removal of secondary metabolites and phytochemicals during the calcination

Table 2: EC_{50} values for ABTS assays of MA-CR_2O_3 NPs, PHE, and standards

ABTS	EC_{50} ± SE (mg·mL^{-1}) (10 min)	EC_{50} ± SE (mg·mL^{-1}) (20 min)	EC_{50} ± SE (mg·mL^{-1}) (30 min)
MA-Cr_2O_3 NPs	4.20 ± 0.04	3.67 ± 0.02	3.39 ± 0.008
PHE	0.09 ± 0.0002	0.087 ± 0.0002	0.084 ± 0.0002
BHT	0.074 ± 0.0001	0.071 ± 0.0002	0.066 ± 0.0001

*This study was conducted in triplicate, with 10, 20, and 30 min of incubation.

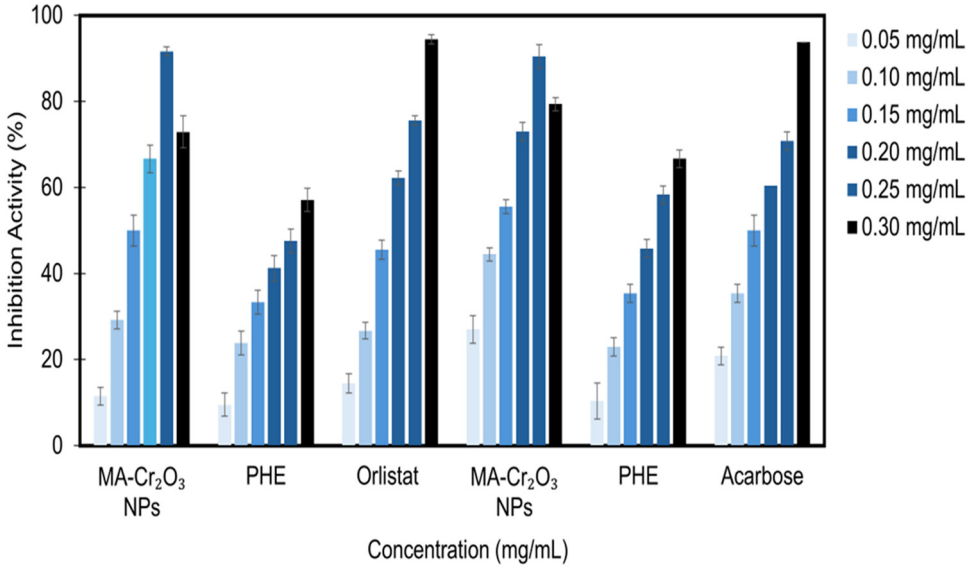

Figure 10: Percentage of inhibition for pancreatic lipase assay and α-amylase assay.

Table 3: EC_{50} values for pancreatic lipase inhibition assay

Pancreatic lipase inhibition	EC_{50} ± SE (mg·mL^{-1})	*p*-Value
MA-Cr_2O_3 NPs	0.16 ± 0.002	>0.05
PHE	0.25 ± 0.01	<0.05
Orlistat	0.16 ± 0.003	—

*This study was conducted in triplicate, with a *p*-value >0.05 for MA-Cr_2O_3 NPs.

Table 4: EC_{50} values for α-amylase inhibition assay

α-amylase inhibition	EC_{50} ± SE (mg·mL^{-1})	*p*-Value
MA-Cr_2O_3 NPs	0.15 ± 0.003	>0.05
PHE	0.21 ± 0.005	<0.05
Acarbose	0.16 ± 0.003	—

*This study was conducted in triplicate, with *p*-value >0.05 for MA-Cr_2O_3 NPs.

process while synthesizing the NPs [54]. Furthermore, the formation of NPs may alter or mask the phytochemicals, affecting the TPC and TFC values [55].

3.3 Free radical scavenging activities

Oxidative stress arises from an imbalance between ROS and antioxidants [56]. This imbalance can lead to various metabolic disorders, including cancer, aging, CVDs, diabetes, obesity, and cell death [57]. Antioxidants are molecules that slow down the oxidation process and neutralize free radicals by donating electrons [58]. DPPH and ABTS are two common methods used to assess antioxidant properties in samples. The DPPH solution is purple, and its decolorization depends on the degree of free radical scavenging activity. This process involves reducing the N-atoms of hydrazine through the transfer of hydrogen atoms from antioxidants [59]. Figure 8 and Table 1 present graphs and data on the percentage and EC_{50} values of DPPH scavenging activities. Ascorbic acid showed the lowest EC_{50} at 60 min, with a value of 0.065 ± 0.0002 mg·mL^{-1}, followed by PHE and MA-Cr_2O_3 NPs. The percentage of DPPH scavenging activity for all samples increased from 30 to 60 min. ABTS+ is a stable free radical chromophore formed by mixing ABTS solution with potassium persulfate. When potassium persulfate oxidizes the ABTS solution, it generates ABTS+, which results in a dark blueish-green chromophore. This chromophore turns light green when reduced by antioxidants [60].

Figure 9 and Table 2 present the graphs and data on the percentage and EC_{50} values of ABTS scavenging activities. Ascorbic acid demonstrated the lowest EC_{50} at 30 min, with a value of 0.066 ± 0.0001 mg·mL^{-1}, followed by PHE and MA-Cr_2O_3 NPs. The percentage of ABTS scavenging activities for all samples increased from 10 to 30 min. Research has shown that metal oxide NPs exhibit antioxidant properties due to the presence of secondary metabolites, such as phenolic compounds, flavonoids, alkaloids, and tannins, which are capped onto the NPs during the synthesis process [61]. Additionally, metal oxide NPs possess free radical scavenging capabilities owing to their inherent physicochemical properties [62].

3.4 Enzyme inhibitions

Pancreatic lipase is an enzyme responsible for breaking down more than 50% of triglycerides in dietary foods into free fatty acids and glycerols. Additionally, α-amylase is another enzyme that helps digest dietary starch into disaccharides and monosaccharides [63]. Both of these processes can eventually contribute to obesity through mechanisms such as adipocyte hypertrophy, hyperplasia, and lipogenesis [64]. Figure 10 presents the inhibition graphs for pancreatic lipase and α-amylase. Tables 3 and 4 show the EC_{50} values for both pancreatic lipase and α-amylase inhibition assays. For pancreatic lipase inhibition, the EC_{50} of MA-Cr_2O_3 NPs is comparable to the standard Orlistat, at 0.16 ± 0.002 and 0.16 ± 0.003 mg·mL^{-1}, respectively. Furthermore, the EC_{50} of MA-Cr_2O_3 NPs for α-amylase inhibition is lower than the standard, acarbose, with values of 0.15 ± 0.003 and 0.16 ± 0.003 mg·mL^{-1}, respectively. In both assays, PHE exhibited the lowest EC_{50} compared to MA-Cr_2O_3 NPs and the standards. MA-Cr_2O_3 NPs showed 91.67% inhibition of pancreatic lipase at 0.2 mg·mL^{-1}, slightly higher than the chemogenic Cr_2O_3 NPs at 0.6 mg·mL^{-1}, which achieved 89.48% inhibition [65]. In the α-amylase assay, MA-Cr_2O_3 NPs demonstrated 90.48% inhibition at 0.2 mg·mL^{-1}, much higher than the reported 26% inhibition at 1 mg·mL^{-1} [35]. The results for MA-Cr_2O_3 NPs show no significant difference compared to the standards, Orlistat, and acarbose, in both pancreatic lipase and α-amylase inhibition assays. This is a positive outcome, as it suggests that MA-Cr_2O_3 NPs are highly comparable to commercial drugs in terms of enzyme inhibition effectiveness and hold promise for future development into potential therapeutic agents.

3.5 MTT assay

Some studies have raised concerns about the toxicity of metal oxide NPs, noting that they can induce toxicity through mechanisms such as oxidative stress and genotoxicity. Additionally, certain metal oxide NPs may have low stability, leading to dissociation and the release of metal ions, which in turn can cause oxidative stress in living organisms [66–68]. In this study, the green synthesis method used to produce NPs aimed to create biocompatible and low-toxicity metal oxide NPs by reducing the use of chemicals and replacing them with phytochemicals derived from pomegranate husk. The results from the MTT assay indicated that the cell viability after treatment with MA-Cr_2O_3 NPs was 55.54 ± 0.003% at a concentration of 0.25 mg·mL^{-1}, while for PHE, the cell viability was 70.32 ± 0.004%. The cytotoxicity of MA-Cr_2O_3 NPs in this study is lower than that reported in other studies, where cell viability was around 50% at a concentration of 0.1 mg·mL^{-1} [69].

4 Conclusions

The successful synthesis of Cr_2O_3 NPs using a microwave-assisted method with PHEs serving as both reducing and capping agents has been demonstrated. Characterization via TEM and scanning electron microscopy (SEM) confirmed that MA-Cr_2O_3 NPs are within the NP size range (<100 nm), fulfilling the criteria for NP classification. Our study revealed significant antioxidant properties of MA-Cr_2O_3 NPs, as shown by DPPH and ABTS assays, highlighting their potential as effective free radical scavengers. Additionally, MA-Cr_2O_3 NPs demonstrated strong inhibition of pancreatic lipase and α-amylase activities, with effectiveness comparable to established standards such as orlistat and acarbose. This suggests that these NPs hold promise for managing lipid and carbohydrate metabolism-related conditions. The cytotoxicity evaluation on Vero cells indicated a cell viability rate exceeding 50% after exposure to the green-synthesized MA-Cr_2O_3 NPs, surpassing values reported in the literature. These findings collectively emphasize the diverse bioactivities of MA-Cr_2O_3 NPs, suggesting their potential as versatile therapeutic agents or functional materials in biomedical applications.

Further investigation into their mechanisms of action and *in vivo* efficacy is necessary to fully explore their clinical and industrial potential. Future research should focus on gaining deeper mechanistic insights and assessing the *in vivo* effects of these NPs to determine their safety and efficacy profiles for potential therapeutic use.

Acknowledgment: We would like to express our gratitude to UTAR for providing the grant (grant number: IPSR/UTARRF/2022-C1/T0) and their facilities and support.

Funding information: Authors state no funding involved.

Author contributions: Shi-Yan Cheah: data curation, formal analysis, investigation, resources, software, validation, visualization, and writing – original draft; Mohammod Aminuzzaman: conceptualization, formal analysis, methodology, project administration, resources, supervision, validation, and writing – review and editing; You-Kang Phang: formal analysis, software, and validation; Sharon Chia-Yen Lim: formal analysis; Ming-Xiu Koh: formal analysis; Sinouvassane Djearamane: resources; Hemaroopini Subramanian: resources; Boon-Hoe Lim: writing

– review and editing; Fang Li: writing – review and editing; Ling-Shing Wong: funding acquisition; Lai-Hock Tey: conceptualization, formal analysis, funding acquisition, methodology, project administration, resources, supervision, validation, and writing – review and editing.

Conflict of interest: Authors state no conflict of interest.

Data availability statement: All data generated or analyzed during this study are included in this published article.

References

[1] Speakman JR. Obesity: The integrated roles of environment and genetics1,2. J Nutr. 2004;134:20905–1055. doi: 10.1093/jn/134.8.2090S.

[2] Boutari C, Mantzoros CS. A 2022 update on the epidemiology of obesity and a call to action: As its twin COVID-19 pandemic appears to be receding, the obesity and dysmetabolism pandemic continues to rage on. Metabolis. 2022;133:e155217. doi: 10.1016/j.metabol.2022.155217.

[3] Cercato C, Fonseca FA. Cardiovascular risk and obesity. Diabetol Metab Syndr. 2019;11:74. doi: 10.1186/s13098-019-0468-0.

[4] Scherer PE, Hill JA. Obesity, diabetes, and cardiovascular diseases: A compendium. Circ Res. 2017;118(11):1703–5. doi: 10.1161/CIRCRESAHA.116.308999.

[5] Ruban A, Stoenchev K, Ashrafian H, Teare J. Current treatments for obesity. Clin Med. 2019;19(3):205–12. doi: 10.7861/clinmedicine.19-3-205.

[6] Dixit VV, Wagh MS. Unfavourable outcomes of liposuction and their management. Indian J Plast Surg. 2013;46(2):377–92. doi: 10.4103/0970-0358.118617.

[7] Bray GA, Heisel WE, Afshin A, Jensen MD, Dietz WH, Long M, et al. The science of obesity management: An endocrine society scientific statement. Endocr Rev. 2018;39(2):79–132. doi: 10.1210/er.2017-00253.

[8] Khan I, Saeed K, Khan I. Nanoparticles: Properties, applications and toxicities. Arab J Chem. 2019;12:908–31. doi: 10.1016/j.arabjc.2017.05.011.

[9] Bayda S, Adeel M, Tucchinardi T, Cordani M, Rizzolio F. The history of nanoscience and nanotechnology: From chemical–physical applications to nanomedicine. Molecules. 2020;25(1):112. doi: 10.3390/molecules25010112.

[10] El-Sheikh S, Mohamed RM, Fouad OA. Synthesis and structure screening of nanostructured chromium oxide powders. J Alloy Compd. 2009;482:302–7. doi: 10.1016/j.jallcom.2009.04.011.

[11] Ying Y, Guan Z, Ofoegbu PC, Clubb P, Rico C, He F, et al. Green synthesis of nanoparticles: Current developments and limitations. Environ Technol Innov. 2022;26:e102336. doi: 10.1016/j.eti.2022.102336.

[12] Huston M, DeBella M, DiBella M, Gupta A. Green synthesis of nanomaterials. Nanomaterials. 2011;11(8):2130. doi: 10.3390/nano11082130.

[13] Lunagariya NA, Patel NK, Jagtap SC, Bhutani KK. Inhibitors of pancreatic lipase: State of the art and clinical perspectives. EXCLI J. 2014;13:897–921. doi: 10.17877/DE290R-6941.

[14] Chikan V, McLaurin EJ. Rapid nanoparticle synthesis by magnetic and microwave heating. Nanomaterials. 2016;6:85. doi: 10.3390/nano6050085.

[15] Ngala RA, Awe MA, Nsiah P. The effects of plasma chromium on lipid profile, glucose metabolism and cardiovascular risk in type 2 diabetes mellitus. A case - control study. PLoS One. 2018;13(7):e197977. doi: 10.1371/journal.pone.0197977.

[16] Monga A, Fulke AB, Dasgupta D. Recent developments in essentiality of trivalent chromium and toxicity of hexavalent chromium: Implications on human health and remediation strategies. J Hazard Mater Adv. 2022;7:e100113. doi: 10.1016/j.hazadv.2022.100113.

[17] Thakur TM, Lokhande RS, Thigle MM, Patil VR. Nanoparticles of chromium oxide by green synthesis using Eucalyptus globulous leaves extract; Characterization and biological activity studies. Mater Today-Proc. 2023;79:100–6. doi: 10.1016/j.matpr.2022.09.368.

[18] Alhalili Z. Metal oxides nanoparticles: General structural description, chemical, physical, and biological synthesis methods, role in pesticides and heavy metal removal through wastewater treatment. Molecules. 2023;28(7):3086. doi: 10.3390/molecules28073086.

[19] Sreekumar S, Sithul H, Muraleedharan P, Azeez JM, Sreeharshan S. Pomegranate fruit as a rich source of biologically active compounds. Biomed Res Int. 2014;2014:686921. doi: 10.1155/2014/686921.

[20] Gachons CP, Breslin PAS. Salivary amylase: Digestion and metabolic syndrome. Curr Diabetes Rep. 2016;16:102. doi: 10.1007/s11892-016-0794-7.

[21] Merino B, Fernández-Díaz CM, Cózar-Castellano I, Perdomo G. Intestinal fructose and glucose metabolism in health and disease. Nutrients. 2020;12(1):94. doi: 10.3390/nu12010094.

[22] Moreno-Indias I, Tinahones FJ. Impaired adipose tissue expandability and lipogenic capacities as ones of the main causes of metabolic disorders. J Diabetes Res. 2015;2015:e970375. doi: 10.1155/2015/970375.

[23] Burton GJ, Jauniaux E. Oxidative stress. Best Pract Res Cl Ob. 2011;25(3):287–199. doi: 10.1016/j.bpobgyn.2010.10.016.

[24] Manna P, Jain SK. Obesity, oxidative stress, adipose tissue dysfunction, and the associated health risks: Causes and therapeutic strategies. Metab Syndr Relat D. 2015;13(10):423–44. doi: 10.1089/met.2015.0095.

[25] Colak E, Pap D. The role of oxidative stress in the development of obesity and obesity-related metabolic disorders. J Med Biochem. 2021;40(1):1–9. doi: 10.5937/jomb0-24652.

[26] Liu QY, Bu ZQ, Yao QF, Ding X, Xia LQ, Huang WT. Microwave-assisted synthesis of chromium oxide nanoparticles for fluorescence biosensing of mercury ions and molecular logic computing. ACS Appl Nano Mater. 2021;4(7):7086–96. doi: 10.1021/acsanm.1c01102.

[27] Nisa FY, Rahman MA, Rafi MKJ, Khan MAN, Sultana F, Majid M, et al. Biosynthesized magnesium oxide nanoparticles from Tamarindus indica seed attenuate doxorubicin-induced cardiotoxicity by regulating biochemical indexes and linked genes. Biomater Adv. 2023;146:e213291. doi: 10.1016/j.bioadv.2023.213291.

[28] Ammulu MA, Viswanath KV, Giduturi AK, Vemuri PK, Mangamuri U, Poda S. Phytoassisted synthesis of magnesium oxide nanoparticles from Pterocarpus marsupium rox.b heartwood extract and its biomedical applications. J Genet Eng Biotechnol. 2021;19(1):1–18. doi: 10.1186/s43141-021-00119-0.

[29] Loganathan S, Shivakumar MS, Karthi S, Nathan SS, Selvam K. Metal oxide nanoparticle synthesis (ZnO-NPs) of Knoxia sumatrensis (Retz.) DC. aqueous leaf extract and it's evaluation of their antioxidant, anti-proliferative and larvicidal activities. Toxicol Rep. 2021;8:64–72. doi: 10.1016/j.toxrep.2020.12.018.
[30] Cam-Van TV, Luu NVH, Nguyen TTH, Nguyen TT, Ho BQ, Nguyen TH, et al. Screening for pancreatic lipase inhibitors: Evaluating assay conditions using p-nitrophenyl palmitate as substrate. Biochem Cell Mol Biol. 2021;15:13–22. doi: 10.1080/26895293.2021.2019131.
[31] Akhter F, Hashim A, Khan MS, Ahmad S, Iqbal D, Srivastava AK, et al. Antioxidant, α-amylase inhibitory and oxidative DNA damage protective property of Boerhaavia diffusa (Linn.) root. S Afr J Bot. 2013;88:265–72. doi: 10.1016/j.sajb.2013.06.024.
[32] Ammerman NC, Beier-Sexton M, Azad AF. Growth and maintenance of vero cell lines. Curr Protoc Microbiol. 2008;4:4E. doi: 10.1002/9780471729259.mca04es11.
[33] Kanagesan S, Hashim M, Tamilselvan S, Alitheen NB, Ismail I, Hajalilou A, et al. Synthesis, characterization, and cytotoxicity of iron oxide nanoparticles. Adv Mater Sci Eng. 2013;2013:710432. doi: 10.1155/2013/710432.
[34] Khan SA, Shahid S, Hanif S, Almoallim HS, Alharbi SA, Sellami H. Green synthesis of chromium oxide nanoparticles for antibacterial, antioxidant anticancer, and biocompatibility activities. Int J Mol Sci. 2021;22(2):e502. doi: 10.3390/ijms22020502.
[35] Iqbal J, Abbasi BA, Munir A, Uddin S, Kanwal S, Mahmood T. Facile green synthesis approach for the production of chromium oxide nanoparticles and their different in vitro biological activities. Microsc Res Techniq. 2020;83(6):706–19. doi: 10.1002/jemt.23460.
[36] Kasprzak MM, Erxleben A, Ochocki J. Properties and applications of flavonoid metal complexes. Rsc Adv. 2015;5:45853–77. doi: 10.1039/C5RA05069C.
[37] Phang YK, Aminuzzaman M, Akhtaruzzaman M, Muhammad G, Ogawa S, Watanabe A, et al. Green synthesis and characterization of CuO nanoparticles derived from papaya peel extract for the photocatalytic degradation of palm oil mill effluent (POME). Sustainability. 2021;13(2):796. doi: 10.3390/su13020796.
[38] Chan YB, Aminuzzaman M, Tey LH, Win YF, Watanabe A, Djearamame S, et al. Impact of diverse parameters on the physicochemical characteristics of green-synthesized zinc oxide–copper oxide nanocomposites derived from an aqueous extract of Garcinia mangostana L. leaf. Materials. 2023;16(15):5421. doi: 10.3390/ma16155421.
[39] Chan YB, Aminuzzaman M, Rahman MK, Win YF, Sultana S, Cheah SY, et al. Green synthesis of ZnO nanoparticles using the mangosteen (Garcinia mangostana L.) leaf extract: Comparative preliminary in vitro antibacterial study. Green Process Synth. 2024;13:e20230251. doi: 10.1515/gps-2023-0251.
[40] Mangangana TP, Makunga NP, Fawole OA, Opara UL. Processing factors affecting the phytochemical and nutritional properties of pomegranate (Punica granatum L.) peel waste: A review. Molecules. 2020;25(20):4690. doi: 10.3390/molecules25204690.
[41] Cheah SY, Tey LH, Aminuzzaman M, Phang YK, Chan YB, Djearamame S, et al. Green synthesis and characterizations of chromium oxide nanoparticles (Cr2O3 NPs) derived from pomegranate husk and its α-amylase inhibitory and antioxidant properties. NHC. 2023;39:51–5. doi: 10.4028/p-od359h.
[42] Hassan D, Khali AT, Solangi AR, El-Mallul A, Shinwari ZK, Maaza M. Physiochemical properties and novel biological applications of Callistemon viminalis-mediated α-Cr2O3 nanoparticles. Appl Organomet Chem. 2019;33:e5041. doi: 10.1002/aoc.5041.
[43] Yasmeen G, Hussain S, Tajammal A, Mustafa Z, Sagir M, Shahid M, et al. Green synthesis of Cr2O3 nanoparticles by Cassia fistula, their electrochemical and antibacterial potential. Arab J Chem. 2013;16(8):e104912. doi: 10.1016/j.arabjc.2023.104912.
[44] Castaño-Rivera P, Calle-Holguín I, Castaño J, Cabrera-Barjas G, Galvez-Garrido K, Troncoso-Ortega E. Enhancement of chloroprene/natural/butadiene rubber nanocomposite properties using organoclays and their combination with carbon black as fillers. Polymers. 2021;13(7):1085. doi: 10.3390/polym13071085.
[45] Hadjiivanov KI, Panayotov DA, Mihaylov MY, Ivanova EZ, Chakarova KK, Andonova SM, et al. Power of infrared and raman spectroscopies to characterize metal-organic frameworks and investigate their interaction with guest molecules. Chem Rev. 2021;121(3):1286–424. doi: 10.1021/acs.chemrev.0c00487.
[46] Karl-Heinz D, O'Brien CP, Mirabella F, Ivars-Barceló a F, Schauermann S. Adsorption of acrolein, propanal, and allyl alcohol on Pd(111): A combined infrared reflection–absorption spectroscopy and temperature programmed desorption study. Phys Chem Chem Phys. 2016;18(20):13960–73. doi: 10.1039/c6cp00877a.
[47] Aziz WJ, Sabry RS, Ali SQ. Green synthesis and characterization of Cr2O3 nanoparticle prepared by using CrCl3.6H2O and roselle extract. AIP Conf Proc. 2022;2398:e020066. doi: 10.1063/5.0094690.
[48] Bradford MC, Konduru MV, Fuentes DX. Preparation, characterization and application of Cr_2O_3/ZnO catalysts for methanol synthesis. FPT. 2003;83(1–3):11–25. doi: 10.1016/S0378-3820(03)00080-8.
[49] Singh J, Jaswal VS, Arora A, Kinger M, Gupta VD. Synthesis and characterization of chromium oxide nanoparticles. Orient J Chem. 2014;30:559–66. doi: 10.13005/ojc/300220.
[50] Chan YB, Selvanathan V, Tey LH, Akhtaruzzaman Md, Anur FH, Djearamane S, et al. Effect of calcination temperature on structural, morphological and optical properties of copper oxide nanostructures derived from Garcinia mangostana L. leaf extract. Nanomaterials. 2022;12(20):3589–608. doi: 10.3390/nano12203589.
[51] Tungmunnithum D, Thongboonyou A, Pholboon A, Yangsabai A. Flavonoids and other phenolic compounds from medicinal plants for pharmaceutical and medical aspects: An overview. Medicines. 2018;5(3):93. doi: 10.3390/medicines5030093.
[52] Mathew S, Abraham TE, Zakaria ZA. Reactivity of phenolic compounds towards free radicals under in vitro conditions. J Food Sci Tech. 2015;52(9):5790–8. doi: 10.1007/s13197-014-1704-0.
[53] Panche AN, Diwan AD, Chandra SR. Flavonoids: An overview. J Nutr Sci. 2016;5:e47. doi: 10.1017/jns.2016.41.
[54] Vera J, Herrera W, Hermosilla E, Díaz M, Parada J, Seabra AB, et al. Antioxidant activity as an indicator of the efficiency of plant extract-mediated synthesis of zinc oxide nanoparticles. Antioxidants. 2023;12(4):784. doi: 10.3390/antiox12040784.
[55] Siakavella IK, Lamari F, Papoulis D, Orkoula M, Gkolfi P, Lykouras M, et al. Effect of plant extracts on the characteristics of silver nanoparticles for topical application. Pharmaceutics. 2020;12(12):1244. doi: 10.3390/pharmaceutics12121244.
[56] Pizzino G, Irrera N, Cucinotta M, Pallio G, Mannino F, Arcoraci V, et al. Oxidative stress: Harms and benefits for human health. Oxid Med Cell Longev. 2017;2017:e8416763. doi: 10.1155/2017/8416763.
[57] Liguori I, Russo G, Curcio F, Bulli G, Aran L, Della-Morte D, et al. Oxidative stress, aging, and diseases. Clin Interv Aging. 2018;13:757–72. doi: 10.2147/CIA.S158513.
[58] Lobo V, Patil A, Phatak A, Chandra N. Free radicals, antioxidants and functional foods: Impact on human health. Pharmacogn Rev. 2010;4(8):118–26. doi: 10.4103/0973-7847.70902.

[59] Baliyan S, Mukherjee R, Priyadarshini A, Vibhuti A, Gupta A, Pandey RP, et al. Determination of antioxidants by DPPH radical scavenging activity and quantitative phytochemical analysis of Ficus religiosa. Molecules. 2022;27(4):1326. doi: 10.3390/molecules27041326.

[60] Zampini IC, Ordoñez RM, Isla MI. Autographic assay for the rapid detection of antioxidant capacity of liquid and semi-solid pharmaceutical formulations using ABTS• + immobilized by gel entrapment. AAPS Pharmscitech. 2010;11(3):1159–63. doi: 10.1208/s12249-010-9484-y.

[61] Marslin G, Siram K, Maqbool Q, Selvakesavan RK, Kruszka D, Kachlicki P, et al. Secondary metabolites in the green synthesis of metallic nanoparticles. Materials. 2018;11(6):940. doi: 10.3390/ma11060940.

[62] Kumar H, Bhardwaj K, Nepovimova E, Kuča K, Dhanjal DS, Bhardwaj S, et al. Antioxidant functionalized nanoparticles: A combat against oxidative stress. Nanomaterials. 2020;10(7):1334. doi: 10.3390/nano10071334.

[63] Ćorković I, Gašo-Sokač D, Pichler A, Šimunović J, Kopjar M. Dietary polyphenols as natural inhibitors of α-amylase and α-glucosidase. Life. 2022;12(11):1692. doi: 10.3390/life12111692.

[64] Bais S, Patel NJ. In vitro anti diabetic and anti obesity effect of J. communis extract on 3T3L1 mouse adipocytes: A possible role of MAPK/ERK activation. Obes Med. 2020;18:e100219. doi: 10.1016/j.obmed.2020.100219.

[65] Cheah SY, Tey LH, Aminuzzaman M, Watanabe A. Chemogenic synthesis of chromium oxide nanoparticles using sol-gel method and its potential on pancreatic lipase inhibition. INTI J. 2022;35:1–8. doi: 10.61453/INTIj.202235.

[66] Jeng HA, Swanson J. Toxicity of metal oxide nanoparticles in mammalian cells. J Environ Sci Heal A. 2006;41(12):2699–711. doi: 10.1080/10934520600966177.

[67] Manuja A, Kumar B, Kumar R, Chhabra D, Ghosh M, Manuja M, et al. Metal/metal oxide nanoparticles: Toxicity concerns associated with their physical state and remediation for biomedical applications. Toxicol Rep. 2021;8:1970–8. doi: 10.1016/j.toxrep.2021.11.020.

[68] Nasim I, Ghani N, Nawaz R, Irfan A, Arshad M, Nasim M, et al. Investigating the impact of carbon nanotube nanoparticle exposure on testicular oxidative stress and histopathological changes in Swiss albino mice. ACS Omega. 2024;9(6):6731–40. doi: 10.1021/acsomega.3c07919.

[69] Alarifi S, Ali D, Alkahtani S. Mechanistic investigation of toxicity of chromium oxide nanoparticles in murine fibrosarcoma cells. Int J Nanomed. 2016;11:1253–9. doi: 10.2147/IJN.S99995.